Available online at www.sciencedirect.com
ScienceDirect
Trans. Nonferrous Met. Soc. China 23(2013) 1589−1594
Transactions of Nonferrous Metals Society of China
www.tnmsc.cn

Low cycle fatigue behavior of extruded AZ31B magnesium alloy

Chang-jian GENG[1], Bao-lin WU[2], Xing-hao DU[2], Yan-dong WANG[1],
Yu-dong ZHANG[2], E. CLAUDE[3], W. FRANCIS[3]

1. Key Laboratory for Anisotropy and Texture of Materials of Ministry of Education, Northeastern University, Shenyang 110819, China;
2. School of Materials Science and Engineering, Shenyang Aerospace University, Shenyang 110136, China;
3. LEM3, University of Metz, 57045 Metz, France

Received 2 May 2012; accepted 8 September 2012

Abstract: The strain-controlled fatigue behavior of an extruded AZ31B magnesium alloy was investigated under symmetric loading at different total strain amplitudes. It is found that except for the low strain magnitude of 0.5%, the alloy exhibits obviously cyclic strain-hardening characteristics during fatigue at strain magnitudes of 0.7%, 0.9%, 1.3% and 1.5%. At the strain of magnitude 0.5%, the alloy exhibits a cyclic hardening characteristic in the initial stage and then a stress constant remaining in the late stage. The hysteresis loop is symmetrical in shape at the strain magnitude of 0.5%, and becomes asymmetrical due to the twinning-detwinning process when the strain magnitude increases. The shape difference of the hysteresis loops between the low and high strain magnitudes was discussed in terms of the differential deformation mechanisms.

Key words: AZ31B magnesium alloy; twinning; dislocation slip; hysteresis loop; cyclic hardening

1 Introduction

Because of their extremely low density in combination with their good castability, workability and damping capacity [1], magnesium and its alloys have been increasingly used in specific structural applications, often replacing aluminum alloys [2]. However, the use of magnesium alloys has been severely limited because of their poor formability at room temperature due to their hexagonal close packed (HCP) structure. In addition, extruded magnesium alloys usually exhibit an intensive anisotropy. The monotonic plastic deformation behavior of wrought magnesium sheets and plates is characterized by strong asymmetry between in-plane tension and compression. This unusual behavior is attributed to the limited number of easy slip systems and the mechanical twinning and detwinning on the $\{10\bar{1}2\}$ planes along the $\langle 10\bar{1}1\rangle$ directions [3]. Generally, deformation modes of Mg and its alloys at room temperatures are basal $\langle a\rangle$ slip, prismatic $\langle a\rangle$ slip, pyramidal $\langle c+a\rangle$ slip, $\{10\bar{1}2\}\langle 10\bar{1}1\rangle$ tension twinning and $\{10\bar{1}1\}\langle 10\bar{1}\bar{2}\rangle$ contraction twinning [4−8]. The tension twinning is a very important deformation mechanism when there is a resolved extension strain parallel to *c*-axis of the deformed grains. So texture has an obvious impact on the deformation mechanisms of magnesium alloys during low cycle fatigue (LCF). In the present study, uniaxial tension-compression fatigue tests were conducted on the extruded AZ31B alloy with {0001} plane parallel to loading axis by strain controlled mode, and the cyclic deformation behavior was investigated throughout the test to examine the hysteresis loops and stress/strain evolution. The mechanism for fatigue behavior evaluation was discussed.

2 Experimental

The AZ31B magnesium alloy used in the present work was received in the form of extruded rod with a diameter of 70 mm. The as-extruded rod was annealed at 793 K for 80 min to remove the residual stress and make a complete recrystallization. The nominal composition of AZ31B alloy is listed in Table 1.

Foundation item: Project (51171120) supported by the National Natural Science Foundation of China; Project (N090202001) supported by the Fundamental Research Funds for the Central Universities, China
Corresponding author: Bao-lin WU; Tel: +86-24-89728701; Fax: +86-24-89728729; E-mail: wubaolin02@yahoo.com.cn
DOI: 10.1016/S1003-6326(13)62635-7

Table 1 Chemical composition of commercial AZ31B alloy (mass fraction, %)

Al	Zn	Si	Cu	Mn	Fe	Ni	Ca	Sn	Mg
2.7	0.96	0.01	≤0.01	0.21	0.002	≤0.001	≤0.01	0.00	Bal.

Specimens for the fatigue testing were machined out of the as-extruded and then annealed rod with the loading axis parallel to the extrusion direction (ED). The strain-controlled fatigue tests were performed using servo-hydraulic Material Test System (MTS Landmark) equipped with a TestStar IIs controller. The strain was applied in triangular waveform (see Fig. 1) with a frequency of 0.5 Hz in laboratory air at room temperature. Five different strain magnitudes ranging from 0.5% to 1.5% were conducted during the fatigue experiment. The strain was measured using an extensometer attached to the sample. For the microstructure observation, the specimen surfaces were ground with SiC papers up to 2000 grit, and then polished with OPS (oxide polishing soluble). Acetic picral solution (4.2 g picric acid, 10 mL acetic acid, 10 mL water, and 70 mL ethanol) was employed to etch the specimens for 10−20 s, which revealed grains and/or twins by optical microscopy. The texture was measured by X-ray back diffraction technique on the longitudinal section of the as-extruded and annealed rod, and presented by {0002} incomplete pole figure. For the transmission electron microscopy observation, the foils were thinned by the twin-jet polishing technique using an electrolyte consisting of 1% $HClO_4$, 99% methanol at 10 V and −40 °C. A JEM−2000EX TEM operated at 200 kV was used for the morphology observation, and a JEOL−JSM−7001F SEM operated at 20 kV was used for EBSD analysis.

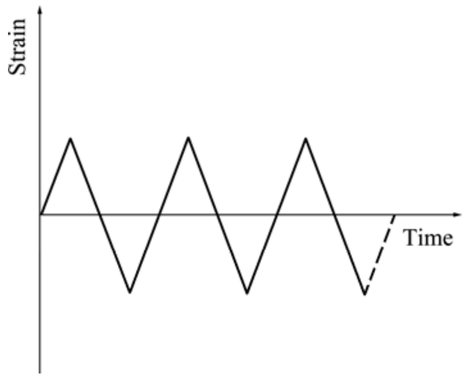

Fig. 1 Schematic diagram of applied strain

3 Results and discussion

3.1 Microstructure and texture

The microstructure of the as-extruded and then annealed rod is shown in Fig. 2. It can be seen that after annealing, the grains are equiaxed with 15 μm in average size.

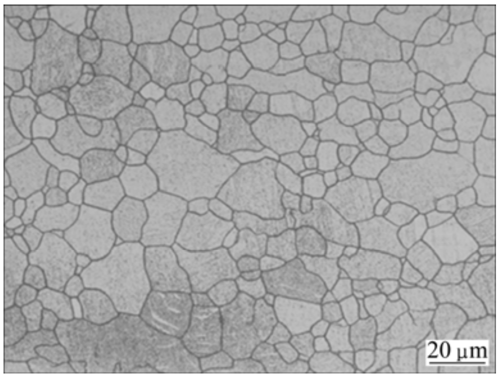

Fig. 2 Optical microstructure of extruded and annealed rod

Figure 3 presents the incomplete {0002} pole figure of the as-extruded and annealed rod. Due to the fact that the texture was measured on any one of the longitudinal sections of the rod and the grain orientation distributes in axial symmetry, the maximum intensity orientations in the {0002} pole figure represent the texture described with the coarse dotted lines in blue color, indicating the ideal orientation distribution locus. It can be seen that the material is highly textured with {0001} basal plane parallel to ED. In this case, both the basal slip and $\{10\bar{1}2\}$ tension twinning in most grains are difficult to be activated under tension, but under compression, $\{10\bar{1}2\}$ tension twinning is extensively convenient to be activated.

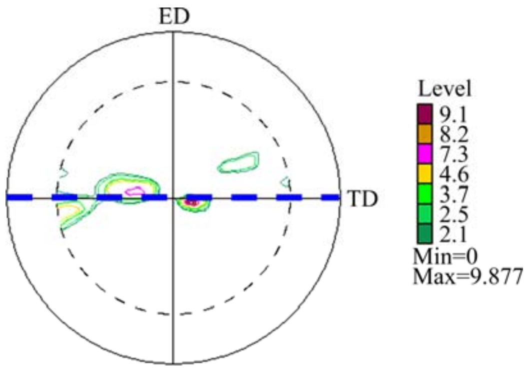

Fig. 3 {0002} pole figure of extruded and annealed rod

3.2 Fatigue properties

Figure 4 shows the relationship of stress amplitude vs the number of cycles. It can be seen from Fig. 4 that as the strain magnitude increases, the stress amplitude increases. Because the high stress usually causes damage to the sample and the crack is affected mainly by tensile stress at a certain strain, fatigue life of the sample at 1.5% strain magnitude with the highest stress is the shortest among all the fatigue samples. And it can be seen that with increasing the number of cycles, except for the sample at 0.5% strain magnitude, a cyclic hardening occurs during the whole fatigue process for all the samples. The sample at 0.5% strain magnitude exhibits a cyclic hardening in the initial period and then a stress constant characteristic. Cyclic strain hardening is generally attributed to the increase of the dislocation density and the dislocation interactions with precipitates during plastic deformation [9]. In addition, grain-boundary sliding (GBS) can contribute to the plastic deformation in a positive manner. It occurs so as to accommodate anisotropic plastic strain and concentrated stresses at the grain-boundaries. The GBS can also produce an additional ⟨*c*⟩ strain component. Local inhomogeneities from grain-to-grain interactions activate limited twinning, particularly in view of the limited number of independent slip systems [10]. The reason that no obvious cyclic hardening at 0.5% strain magnitude was observed in the later fatigue period may be related to the GBS and the anelasticity under the very low strain instead of the dislocation slips. As strain magnitude increases, dislocation slips and the tension twinning activate, resulting in the cyclic hardening. Fatigue crack initiation was dominantly induced by dislocation slips at lower strain magnitudes and by twinning-detwinning process at higher strain magnitudes [11].

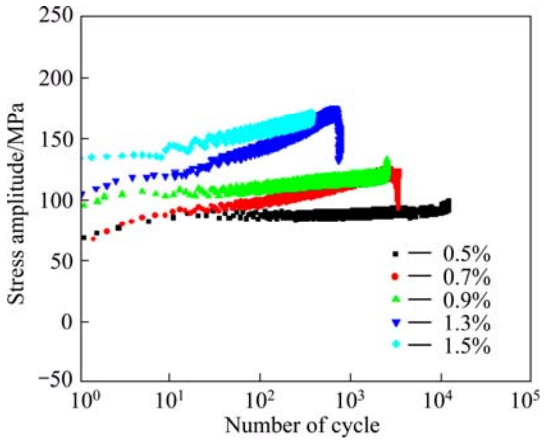

Fig. 4 Stress amplitude vs number of cycle (N) at different strains

The total strain amplitude $\Delta\varepsilon_t$ can be expressed as the sum of total elastic strain amplitude $\Delta\varepsilon_e$ and plastic strain amplitude $\Delta\varepsilon_p$:

$$\Delta\varepsilon_t/2=\Delta\varepsilon_e/2+\Delta\varepsilon_p/2 \quad (1)$$

The elastic strain amplitude can be replaced by the Basquin equation:

$$\Delta\varepsilon_e/2=\sigma'_f\,(2N_f\,)^b/E \quad (2)$$

where σ'_f is the fatigue strength coefficient; b is the fatigue strength exponent, $2N_f$ is the number of reversals to failure, and E is the elastic modulus. Also, the plastic strain amplitude can be expressed in terms of the Coffin-Manson law:

$$\Delta\varepsilon_p/2=\varepsilon'_f(2N_f)^c \quad (3)$$

where ε'_f is the fatigue ductility coefficient and c is the fatigue ductility exponent.

The curves of elastic strain amplitude vs the number of reversals to failure and plastic strain amplitude vs the number of reversals to failure are given in Fig. 5, where the values of strain amplitudes are taken from the half-life hysteresis loops. By the apparent linear fit, the values of σ'_f=495 MPa, b=−0.18, ε'_f=3.1 and c=−0.4 are obtained. They are approximate with the values of the fatigue of AZ31 alloy reported in the previous research [12].

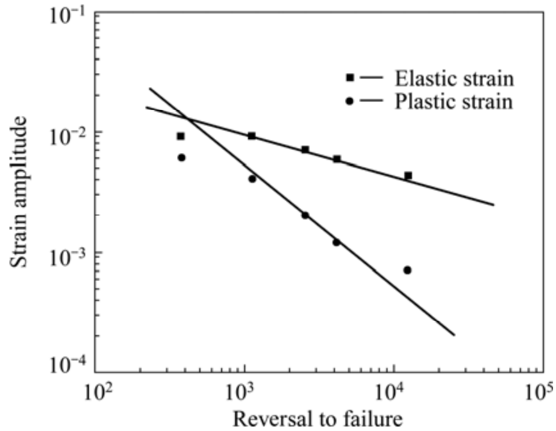

Fig. 5 Relationship between strain amplitude at half-life and number of reversals to failure ($2N_f$)

Figure 6 shows the hysteresis loops at the 100th cycle at strain magnitude ranging from 0.5% to 1.5%. It is interesting to note that except for the sample at 0.5% strain magnitude, the loops are asymmetric, distorted at the tensile region, which is attributed to the texture with {0001} basal plane parallel to ED. The shape of the hysteresis loops depends significantly on the strain amplitude indicated by CACERES et al [13], MANN et al [14] and MURÁNSKY et al [15]. The maximum stress increases and the distorted region becomes widespread with strain amplitude increasing due to activation of a twinning– detwinning process.

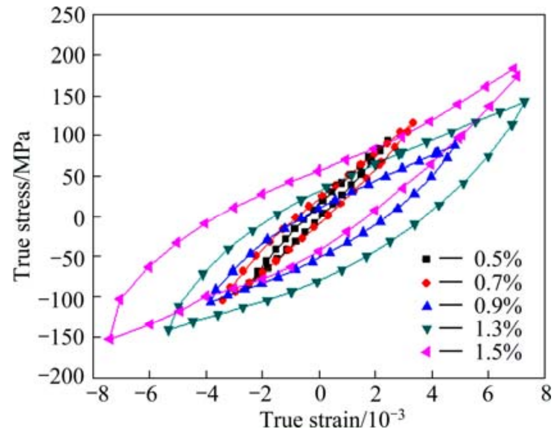

Fig. 6 True stress—true strain hysteresis loops at different strain magnitudes

Figure 7 shows the true stress—true strain hysteresis loops of the sample at strain magnitude of 0.9% before the 547th cycle. The maximum tensile stress increases with cycle number increasing as indicated by arrows 1 and 2 in Fig. 7(a), while the maximum compressive stress maintains nearly the same. This means that the cyclic hardening mainly results from tensile stage in a cyclic deformation, in which dislocation slip interaction is responsible for hardening. With the cyclic number increasing, the shape of hysteresis loops changes as shown in Fig. 7(b). This could be explained as cracks generation. During strain alternation in one loop, the stress decreases when the strain reaches the maximum during both tension and compression. It seems to be related to the crack activation which would induce stress decreasing. Due to the fact that the alloy has the texture with {0001} basal plane parallel to loading axis, the resolved shear stress for basal slip is so low that this slip cannot be activated in most grains, and the plastic deformation during compression is dominantly accommodated by $\{10\bar{1}2\}$ tension twinning because of its lowest critical resolved shear stress (CRSS) compared with the other deformation modes. The maximum compressive stress is changeless as shown in Fig. 7(a). This demonstrates that the maximum compressive stress is not affected evidently by repeating strain resulting from the tension twinning. However, it should be noted that during tensile deformation, some $\{10\bar{1}2\}$ tension twins are remained after detwinning. In post-detwinning deformation, prismatic ⟨*a*⟩ slip and pyramidal ⟨*c*+*a*⟩ slip are needed to compensate the residual strain [16]. In this case, the contraction twinning is not much convenient to be activated because of its CRSS much higher than those of the prismatic and pyramidal slips. Therefore, as compared with the compression process, deformation strain in the tensile process is easy to result in strain hardening due to the dislocation interactions. Consequently, the hysteresis loops are usually asymmetric in the fatigue process with respect to the loading direction alternation due to the difference of deformation modes. As cyclic number and strain accumulation increases, cracks generate to change the loops shape (Fig. 7(b)).

Figure 8 shows the distribution of misorientation angle in the deformed microstructures of the sample at 1.5% strain magnitude at 3/4 cycle and 5/4 cycle, respectively. It can be seen that there are many $\{10\bar{1}2\}$ tension twins in 3/4 cycle deformed sample, further tensile deformation makes tension twins reduce in number as seen from Fig. 8. Accordingly, it is reasonable to suggest that twinning-detwinning process is easy to

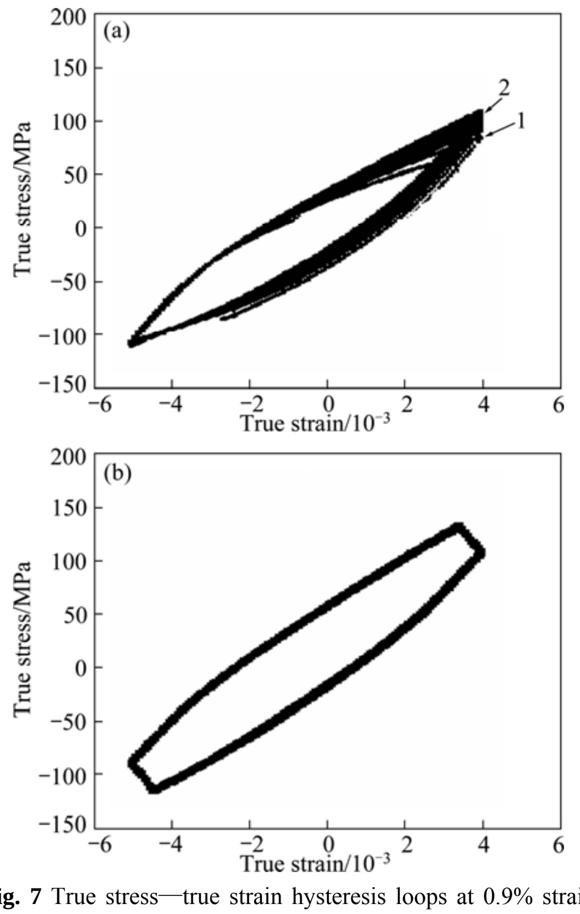

Fig. 7 True stress—true strain hysteresis loops at 0.9% strain magnitude: (a) Before 547th cycle; (b) 547th to 2066th cycle

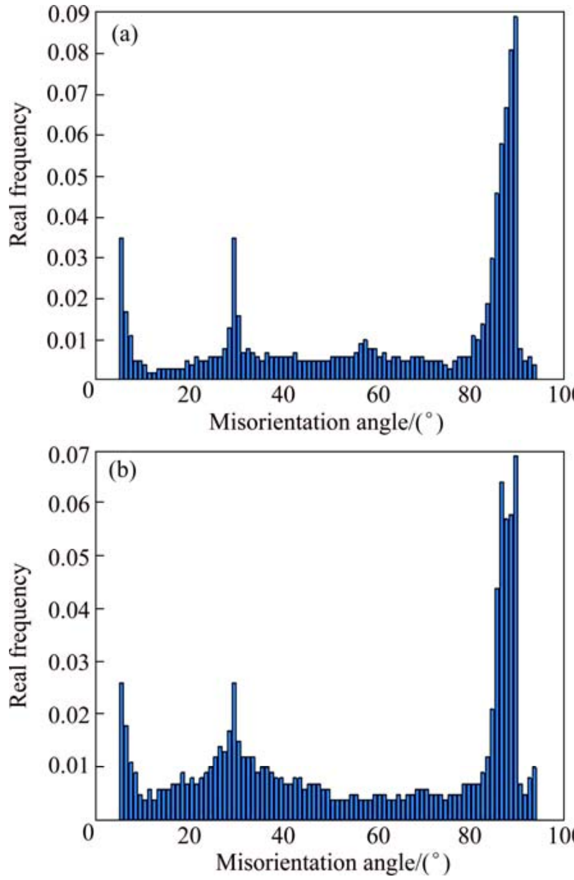

Fig. 8 Distribution of misorientation angle in microstructures of samples deformed at 1.5% strain magnitude with different cycles: (a) 3/4 cycle; (b) 5/4 cycle

occur during cyclic deformation. ZENNER and RENNER [17] suggested that the asymmetry in tensile and compressive deformation of magnesium alloy mainly depends on the texture of materials, and on the difference in the initiation stress of twinning under tensile and compressive yielding. On the other hand, ZHOU et al [18] put forward the hysteresis effect attributing to the formation of fully reversible dislocation-based incipient kink bands.

Figure 9 shows TEM images of fractured LCF samples at low and high strain magnitudes, respectively. It can be seen that there are many dislocations in the sample at low strain magnitude as shown in Fig. 9(a), but there are simultaneously twins and dislocations in the sample at high strain magnitude as shown in Fig. 9(b). So it is believed that in addition to dislocation slips, cyclic deformation at higher strain magnitude is dominated by twinning-detwinning, whereas at lower strain magnitude deformation is dominated by dislocation slips.

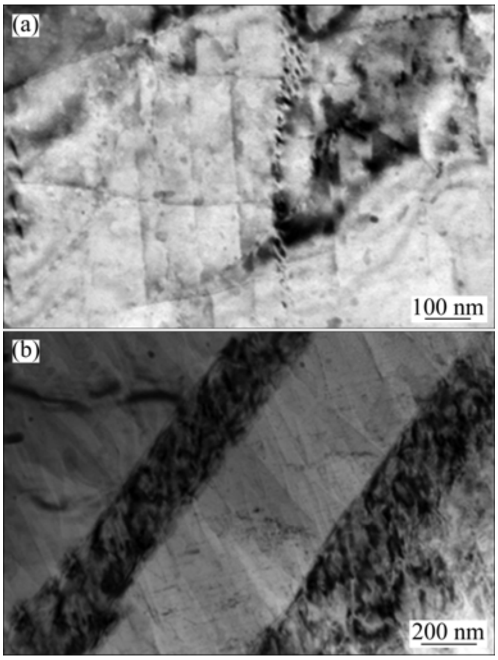

Fig. 9 TEM images of fractured extruded AZ31B magnesium alloy: (a) 0.5% strain magnitude; (b) 1.5% strain magnitude

4 Conclusions

1) Under the symmetric loading, the textured AZ31B magnesium alloy exhibits cyclic strain-hardening characteristics in the range of strain magnitude from 0.7% to 1.5%.

2) At low strain magnitude of 0.5%, the alloy exhibits the cyclic hardening in the initial period and then the stress remains constant in the late period.

3) LCF plastic deformation at high strain magnitude is dominated by twinning-detwinning and dislocation, whereas it is dominated by dislocations and then grain boundary sliding at low strain magnitude.

4) The hysteresis loop is symmetrical in shape at the low strain magnitude of 0.5%, and becomes asymmetrical at high strain magnitudes due to the tension twinning in compression and subsequent detwinning in tensile process.

References

[1] AVEDESIAN M M, BAKER H. ASM specialty handbook: Magnesium and magnesium alloys [M]. ASM International, 1999.

[2] SANDERS P G, KESKE J S, LEONG K H, KOMECKI G. High power Nd:YAG and CO_2 laser welding of magnesium [J]. J Laser Appl, 1999, 11(2): 96−103.

[3] AGNEW S R, DUYGULU O. Plastic anisotropy and the role of non-basal ship in magnesium alloy [J]. Int J Plasticity, 2005, 21: 1161−1193.

[4] KOIKE J, OHYAMA R. Geometrical criterion for the activation of prismatic slip in AZ61 Mg alloy sheets deformed at room temperature [J]. Acta Mater, 2005, 53: 1963−1972.

[5] KOIKE J, KOBAYASHI T, MUKAI T, WATANABE H, SUZUKI M, MARUYAMA K, HIGASHI K. The activity of non-basal slip systems and dynamic recovery at room temperature in fine-grained AZ31B magnesium alloys [J]. Acta Mater, 2003, 51: 2055−2065.

[6] KESHAVARZ Z, BARNETT M R. Observation of deformation modes in Mg−3Al−1Zn [J]. Materials Forum, 2005, 29: 382−386.

[7] KOIKE J. Enhanced deformation mechanisms by anisotropic plasticity in polycrystalline Mg alloys at room temperature [J]. Metallurgical and Materials Transaction A, 2005, 36: 1689−1695.

[8] JIANG L, JONAS J J, LUO A A, SACHDEV A K, GODET S. Twinning-induced softening in polycrystalline AM30 Mg alloy at moderate temperatures [J]. Scripta Materialia, 2006, 54: 771−775.

[9] CHEN L, WANG C, WU W, LIU Z, GRIGORETA M, STOICA M, WU L, LIAW P K. Low-cycle fatigue behavior of an as-extruded AM50 magnesium alloy [J]. Metallurgical and Materials Transaction A, 2007, 38(13): 2235−2241.

[10] LOU X Y, LI M, BOGER R K, AGNEW S R, WAGONER R H. Hardening evolution of AZ31B Mg sheet [J]. International Journal of Plasticity, 2007, 23: 44−86.

[11] LI Q Z, YU Q, ZHANG J X, JIANG Y Y. Effect of strain amplitude on tension–compression fatigue behavior of extruded Mg6Al1ZnA magnesium alloy [J]. Scripta Materialia, 2010, 62: 778−781.

[12] LI F, WANG Y, CHEN L J, LIU Z. Low-cycle fatigue behavior of two magnesium alloys [J]. Journal of Materails Science, 2005: 1529−1531.

[13] CACERES C. Pseudoelastic behaviour of cast magnesium AZ91 alloy under cyclic loading-unloading [J]. Acta Mater, 2003, 51: 6211−6218.

[14] MANN G, SUMITOMO T, CACERES C, GRIFFITHS J. Reversible plastic strain during cyclic loading–unloading of Mg and Mg−Zn alloys [J]. Mater Sci Eng A, 2007, 456: 138−46.

[15] MURANSKY O, CARR D G, ŠITTNER P, OLIBER E C. In situ neutron diffraction investigation of deformation twinning and pseudoelastic-like behaviour of extruded AZ31 magnesium alloy [J]. Int J Plast, 2009, 25: 1107−1127.

[16] WU L, JAIN A, BROWN D W, STOICA G M, AGNEW S R, CLAUSEN B, FIELDEN D E, LIAW P K, Twinning-detwinning

behavior during the strain-controlled low-cycle fatigue testing of a wrought magnesium alloy ZK60A [J]. Acta Mater, 2008, 56: 688−695.

[17] ZENNER H, RENNER F. Cyclic material behavior of magnesium die castings and extrusions [J]. Int J Fatigue, 2002, 24: 1255−1260.

[18] ZHOU A, BASU S, BARSOUM M. Kinking nonlinear elasticity, damping, microyielding of hexagonal close-packed metals [J]. Acta Mater 2008, 56: 60−67.

挤压 AZ31B 镁合金的低周疲劳性能

耿长建[1]，武保林[2]，杜兴蒿[2]，王沿东[1]，张宇东[2]，E. CLAUDE[3], W. FRANCIS[3]

1. 东北大学 材料各向异性与织构教育部重点实验室，沈阳 110819；
2. 沈阳航空航天大学 材料科学与工程学院，沈阳 110136；
3. LEM3, University of Metz, 57045 Metz, France

摘　要：通过外加总应变幅控制的拉−压对称疲劳试验，研究常温下挤压 AZ31B 镁合金在不同应变幅下的疲劳性能。结果表明，除了在低应变幅 0.5%外，样品均呈现循环应变硬化；应变幅为 0.5%时，样品在初始阶段呈现循环硬化，随后保持应力恒定；在压缩过程中孪晶的产生以及随后的卸载和反向拉伸过程中的去孪晶行为导致了高应变幅下的滞回环形状拉−压不对称现象，而低应变幅 0.5%下的滞回环形状基本对称，说明低应变幅下孪生−去孪生现象不明显。在整个疲劳过程中，高应变和低应变下的应力—应变曲线呈现 2 种不同的滞回环形状，这是由不同疲劳阶段孪生和位错滑移 2 种不同的变形机制所导致。

关键词：AZ31B 镁合金；孪晶；位错滑移；滞回曲线；循环硬化

(Edited by Xiang-qun LI)